Molecular Therapy
Original Article

Local Delivery of miR-21 Stabilizes Fibrous Caps in Vulnerable Atherosclerotic Lesions

Hong Jin,[1,7] Daniel Y. Li,[2,3,7] Ekaterina Chernogubova,[1] Changyan Sun,[1] Albert Busch,[2,3] Suzanne M. Eken,[1] Peter Saliba-Gustafsson,[1] Hanna Winter,[1] Greg Winski,[1] Uwe Raaz,[4] Isabel N. Schellinger,[4] Nancy Simon,[1] Renate Hegenloh,[2,3] Ljubica Perisic Matic,[5] Maja Jagodic,[6] Ewa Ehrenborg,[1] Jaroslav Pelisek,[2,3] Hans-Henning Eckstein,[2,3] Ulf Hedin,[5] Alexandra Backlund,[1] and Lars Maegdefessel[1,2,3]

[1]Department of Medicine, Karolinska Institute, Stockholm, Sweden; [2]Department of Vascular and Endovascular Surgery, Technical University Munich, Munich, Germany; [3]German Center for Cardiovascular Research (DZHK), Munich, Germany; [4]University Heart Center, Göttingen, Germany; [5]Department of Molecular Medicine and Surgery, Karolinska Institute, Stockholm, Sweden; [6]Department of Clinical Neuroscience, Karolinska Institute, Stockholm, Sweden

miRNAs are potential regulators of carotid artery stenosis and concordant vulnerable atherosclerotic plaques. Hence, we analyzed miRNA expression in laser captured micro-dissected fibrous caps of either ruptured or stable plaques (n = 10 each), discovering that miR-21 was significantly downregulated in unstable lesions. To functionally evaluate miR-21 in plaque vulnerability, *miR-21* and *miR-21*/apolipoprotein-E double-deficient mice (*Apoe*$^{-/-}$*miR-21*$^{-/-}$) were assessed. *miR-21*$^{-/-}$ mice lacked sufficient smooth muscle cell proliferation in response to carotid ligation injury. When exposing *Apoe*$^{-/-}$*miR-21*$^{-/-}$ mice to an inducible plaque rupture model, they presented with more atherothrombotic events (93%) compared with *miR-21*$^{+/+}$*Apoe*$^{-/-}$ mice (57%). We discovered that smooth muscle cell fate in experimentally induced advanced lesions is steered via a REST-miR-21-REST feedback signaling pathway. Furthermore, *Apoe*$^{-/-}$*miR-21*$^{-/-}$ mice presented with more pronounced atherosclerotic lesions, greater foam cell formation, and substantially higher levels of arterial macrophage infiltration. Local delivery of a miR-21 mimic using ultrasound-targeted microbubbles into carotid plaques rescued the vulnerable plaque rupture phenotype. In the present study, we identify miR-21 as a key modulator of pathologic processes in advanced atherosclerosis. Targeted, lesion site-specific overexpression of miR-21 can stabilize vulnerable plaques.

INTRODUCTION

Although tremendous efforts have been put into prevention and treatment of atherosclerosis and its related diseases, plaque rupture followed by myocardial infarction or ischemic stroke remains the major cause of mortality and morbidity in our aging society worldwide.[1,2] In the clinical setting, the identification and efforts aiming at the stabilization of unstable advanced atherosclerotic lesions in the carotid artery prone to rupture and inducing an ischemic stroke are of utmost importance.[3] Vulnerable plaques are considered as lesions with thinned-out fibrous caps, due to a limited amount of viable smooth muscle cells (SMCs), overlaying a lipid-rich necrotic core, containing inflammatory infiltrates and macrophages. Intra-plaque hemorrhages, neo-angiogenesis, and an obstructed lumen with a visible adhering thrombus complete the features of an unstable, ruptured plaque.[4–6] Currently the most effective treatment option for rupture-prone and essentially ruptured plaques in the carotid artery remains endarterectomy of the lesion through an open surgical approach.[7] As advanced imaging technology of vulnerable plaques has brought us closer to detecting rupture-prone lesions before an actual clinical event occurs,[3,8,9] treatment strategies targeted at "plaque sealing" appear generally interesting and potentially promising.

In recent years, microRNAs (miRNAs; short RNAs consisting of 18–25 nucleotides) have received much attention in their role as crucial mediators of disease exacerbation, as both biomarkers and potential therapeutic targets. miRNAs inhibit gene expression via direct and complementary binding to the 3′UTR site of mRNAs, causing translational repression and/or degradation.[10] Previous studies from our research group have revealed a key role for miR-21 as a regulator of SMC dynamics, including apoptosis and proliferation in experimental models of aortic aneurysms and restenosis.[11,12] miR-21 is generally known for its considerably high expression values and regulatory role in the cardiovascular system.[13]

The aim of the present study was to investigate miRNAs with importance to fibrous cap stability in advanced atherosclerotic lesions, both in human carotid artery endarterectomy specimens and in experimental murine models of vascular remodeling and inducible plaque rupture. We identified miR-21 as a potential therapeutic target to stabilize experimentally induced plaques through enhancement of SMC

Received 1 August 2017; accepted 12 January 2018;
https://doi.org/10.1016/j.ymthe.2018.01.011.

[7]These authors contributed equally to this work.

Correspondence: Lars Maegdefessel, Vascular Biology Unit, Department of Vascular and Endovascular Surgery, Klinikum rechts der Isar der Technical University Munich, Ismaninger Strasse 22, 81675 Munich, Germany.
E-mail: lars.maegdefessel@tum.de

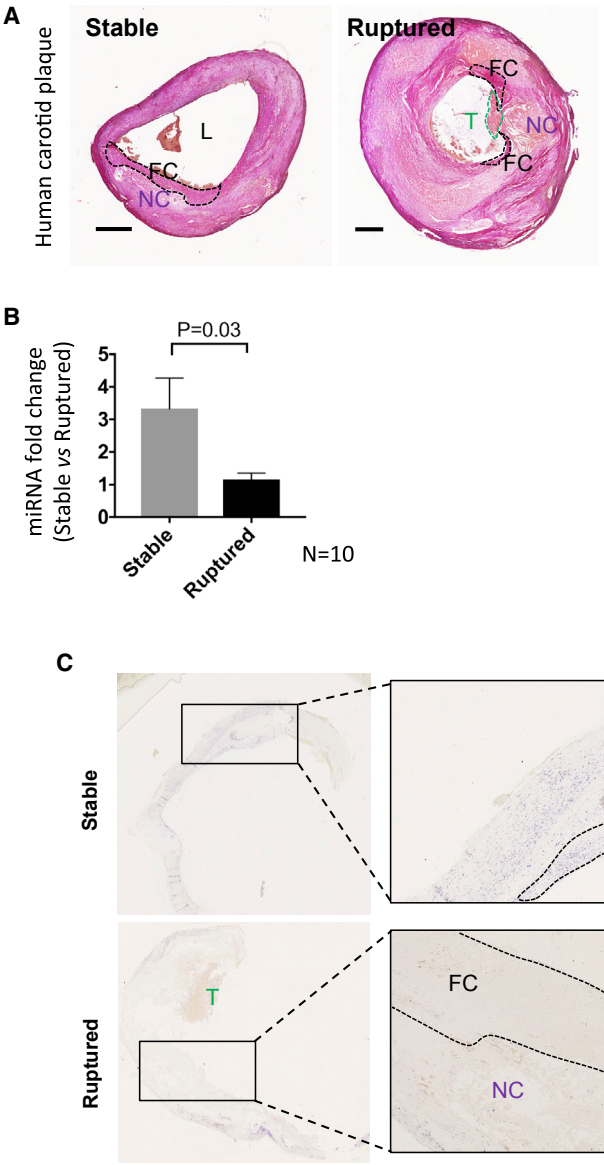

Figure 1. Decreased miR-21 Expression Is Associated with Atherosclerotic Fibrous Cap Instability and Rupture

(A) Staining for laser captured fibrous caps of ten ruptured versus ten stable human carotid atherosclerotic plaques. FC, fibrous cap; L, lumen; NC, necrotic core; T, thrombus. (B) qRT-PCR analysis shows significant miR-21 downregulation in ruptured versus stable plaques (mean + SEM). Groups were compared using Student's t test. (C) *In situ* hybridization (ISH) of human carotid arteries indicate that miR-21 is expressed in the intima-media, as well as fibrous cap structures of stable plaques, whereas it appears reduced in ruptured lesions. *$p < 0.05$ versus stable. Bar, 100 μm.

proliferation rates and inhibition of macrophage activity. We applied delivery tools to locally enhance uptake of miR-21 in carotid lesions, allowing us to enhance a distinctive uptake, while limiting off-target effects in other organ systems.

RESULTS

Reduced miR-21 Levels in Carotid Atherosclerotic Plaque Fibrous Caps in Symptomatic Patients

To specifically detect miRNAs with implications for acute plaque rupture events, we performed micro-dissection laser capture on samples of advanced carotid artery disease from the Munich Vascular Biobank (Figure 1A). Patient samples were matched for age, gender, and risk profile. Two groups were compared: ten plaques with histomorphologically detected features of a ruptured plaque from symptomatic patients (stroke or transient ischemic attack [TIA] within the past >14 days) versus ten specimens of stable lesions from asymptomatic patients (high-grade stenosis; Figure 1A). Plaques were classified as ruptured or stable according to the American Heart Association (AHA) classification after Stary et al.[14] and based on fibrous cap thickness (<200 or >200 μm) as proposed by Redgrave et al.[15] Apart from miR-210, which we have previously reported as being significantly downregulated in locally drawn plasma from advanced lesions, and affecting plaque vulnerability via the tumor suppressor gene adenomatous polyposis coli (Apc) and the canonical Wnt pathway,[16] miR-21 was identified as the only other miRNA that is significantly deregulated (repressed) in fibrous caps from ruptured versus stable lesions (Figure 1B). Reduced miR-21 levels in ruptured human plaque specimens were further confirmed using *in situ* hybridization for miR-21 (Figure 1C). On the basis of *in situ* hybridization and immunohistochemical analysis for smooth muscle cell α-actin (SMA), miR-21 seemed to be predominantly expressed in SMCs of the intima-media as well as in the fibrous cap of advanced lesions (Figure S1).

miR-21 Depletion Suppresses Neointima Formation and Enhances Plaque Instability

miR-21$^{-/-}$ mice on a C57BL/6 background underwent the well-established complete ligation model in the common carotid artery for 4 weeks, enabling us to study the effect of miR-21 depletion during vascular (inward) remodeling and development of myointimal hyperplasia. *miR-21*$^{-/-}$ mice displayed a dramatic decrease in neointima formation and overall SMC content compared with wild-type (WT) littermate controls (n = 5 per group; Figure 2A). To further functionally evaluate the contribution of miR-21 to actual plaque vulnerability, we generated *Apoe*$^{-/-}$*miR-21*$^{-/-}$ mice, again on a C57BL/6

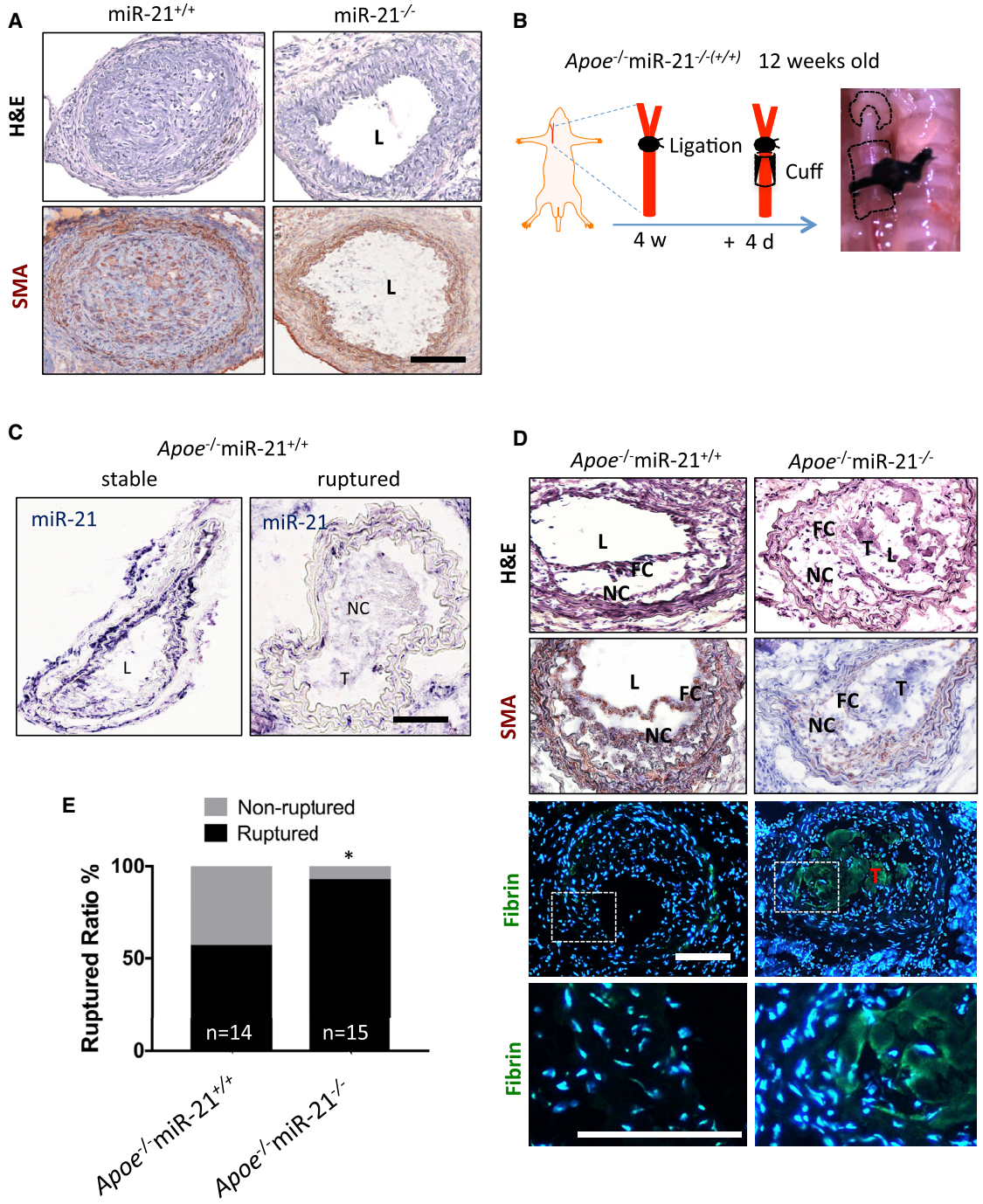

Figure 2. miR-21 Deficiency Suppresses Neointima Formation and Fibrous Cap Stability in Mouse Models of Advanced Atherosclerosis

(A) Histologic images stained with H&E and smooth muscle cell α-actin (SMA) of the right common carotid artery (300 μm from the site of complete ligation). (B) Descriptive cartoon of the mouse carotid plaque rupture model. Male *Apoe*-deficient mice, 12 weeks of age, receive an incomplete carotid artery ligation directly below the bifurcation. Within 4 weeks, a plaque forms proximal to the ligation. Placement of a cast with a conically shaped internal lumen results in plaque rupture in about 50%–60% of $Apoe^{-/-}$ mice. (C) ISH of right carotid arteries from *Apoe*-deficient mice shows significantly decreased miR-21 expression in ruptured versus stable plaques. (D) Histologic images stained with H&E, α-SMA, and cross-linked fibrin of stable and ruptured carotid plaques in $Apoe^{-/-}miR\text{-}21^{+/+}$ and $Apoe^{-/-}miR\text{-}21^{-/-}$ mice. FC, fibrous cap; L, lumen; NC, necrotic core; T, thrombus. (E) $Apoe^{-/-}miR\text{-}21^{-/-}$ mice (n = 15) display significantly higher plaque rupture rates compared with $Apoe^{-/-}miR\text{-}21^{+/+}$ mice (n = 14) ($p = 0.02$). Data were analyzed using chi-square or Fisher's exact test. *$p < 0.05$ versus $Apoe^{-/-}miR\text{-}21^{+/+}$. Bar, 100 μm.

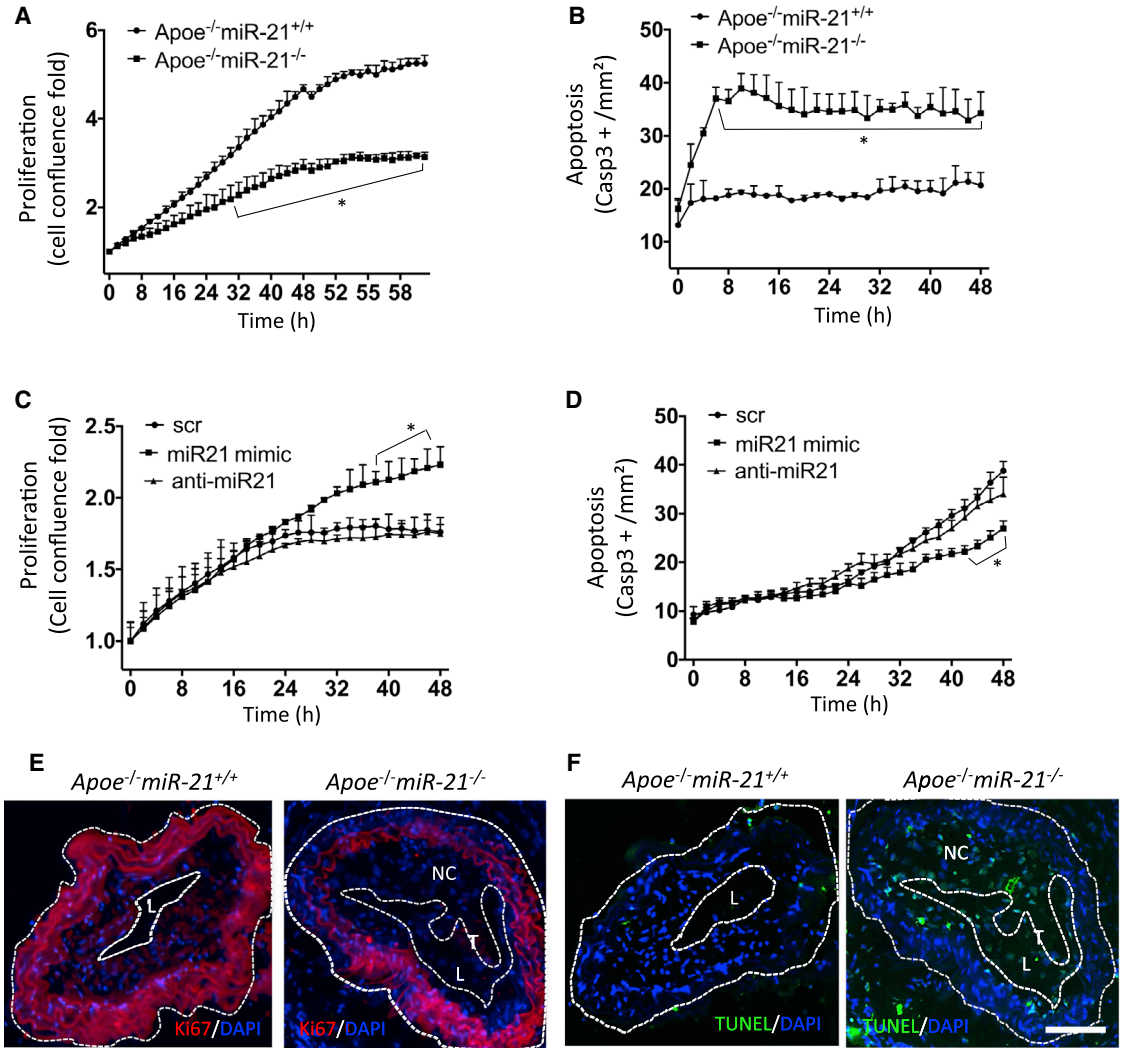

Figure 3. miR-21 Deficiency Limits SMC Proliferation While Enhancing Apoptosis

(A) Substantially suppressed proliferation of cultured primary aortic SMCs from *Apoe*$^{-/-}$*miR-21*$^{-/-}$ mice compared with cells from *Apoe*$^{-/-}$*miR-21*$^{+/+}$ littermate controls (n = 3 per group). Proliferation is indicated as percentage of confluence and plotted as fold increase (percentage confluence at specific time divided by percentage confluence at time point 0). (B) Enhanced apoptosis of primary aortic SMCs from *Apoe*$^{-/-}$*miR-21*$^{-/-}$ mice. (C) miR-21 mimic treatment stimulates human carotid SMC proliferation significantly. (D) miR-21 mimic significantly inhibits HCtASMC apoptosis. (E) Ki-67 immunofluorescence staining confirms decreased proliferation in the carotid plaque of *Apoe*$^{-/-}$*miR-21*$^{-/-}$ mice. L, lumen; NC, necrotic core. (F) Increased SMC apoptosis assessed in the carotid plaque of *Apoe*$^{-/-}$*miR-21*$^{-/-}$ mice by using the TUNEL assay. *$p < 0.05$ versus Apoe$^{-/-}$miR-21$^{+/+}$ or SCR. Mean ± SEM. Bar, 100 μm. For (A)–(D), data were obtained from two experiments run in duplicates. For (E) and (F), data were obtained from two experiments run in triplicate. Data presented in (A)–(D) were analyzed using two-way repeated-measures ANOVA.

background. Mice were exposed to the previously described inducible plaque rupture model (Eken et al.[16]), using incomplete ligation of the common carotid artery with consecutive cuff placement proximal to the ligated region (Figure 2B). Consistent with human plaques, miR-21 expression was generally reduced in ruptured versus stable plaques of *Apoe*$^{-/-}$ mice (Figure 2C). More important, *Apoe*$^{-/-}$*miR-21*$^{-/-}$ mice presented with substantially increased rupture rates and detected atherothrombotic events (n = 15 [93%]) compared with *Apoe*$^{-/-}$*miR-21*$^{+/+}$ littermate controls (n = 14 [57%]), which was confirmed on the basis of histology (H&E), SMA-positive cells, and fibrin staining of the adhering thrombus upon plaque rupture (Figures 2D and 2E). Furthermore, we were able to detect decreased proliferation (on the basis of Ki-67-positive immunofluorescent cells) and an increase in apoptotic signaling (indicated through TUNEL assay staining), mainly in fibrous cap structures of *Apoe*$^{-/-}$*miR-21*$^{-/-}$ mice versus littermate miR-21 non-depleted control animals (Figures 3E and 3F).

miR-21 Deficiency Leads to an Imbalance of SMC Proliferation and Apoptosis

To directly observe the effect of miR-21 modulation on proliferation and apoptosis of SMCs, we isolated primary aortic SMCs from

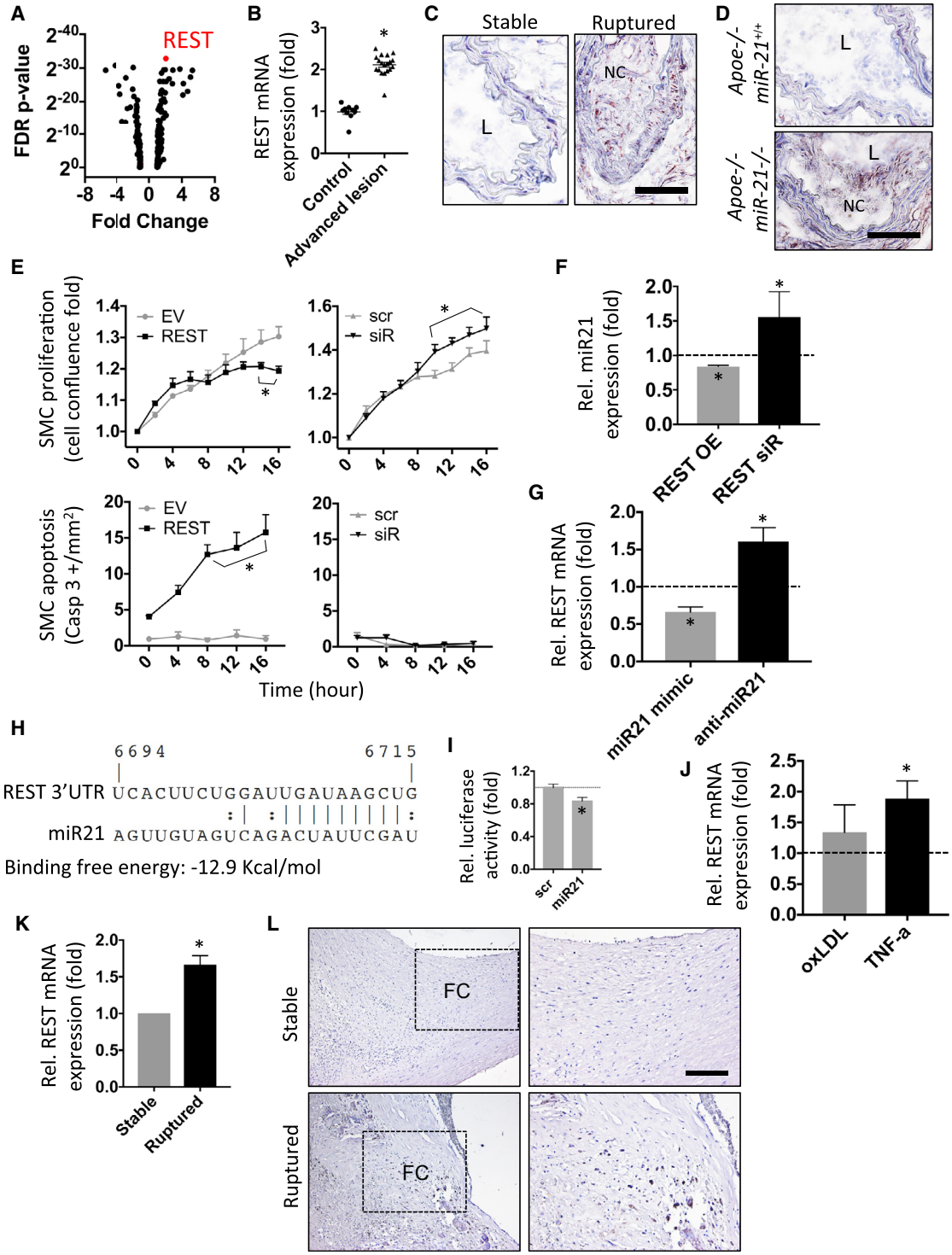

Figure 4. REST-miR-21 Feedback Loop Regulates SMC Fate

(A) Mouse transcriptome array (MTA) profiling data shows significant upregulation of REST in advanced carotid artery plaques compared with uninjured control arteries; FDR p value is expressed as binary logarithm. (B) REST mRNA expression is significantly upregulated in advanced lesion material compared with control carotid artery. (C) Increased REST protein levels in ruptured carotid plaques of male *Apoe*-deficient mice assessed with REST IHC staining. L, lumen; NC, necrotic core. (D) REST IHC staining indicates higher REST levels in the carotid artery and plaques of *Apoe*$^{-/-}$*miR-21*$^{-/-}$ mice. (E) REST overexpression with plasmid transfection suppresses proliferation

(legend continued on next page)

age-matched 6-week-old *Apoe*$^{-/-}$*miR-21*$^{+/+}$ and *Apoe*$^{-/-}$*miR-21*$^{-/-}$ littermate mice. Consistent with the striking increase in plaque rupture, limited proliferation, and enhanced death signaling *in vivo*, arterial SMCs from miR-21-depleted mice presented with halted cellular proliferation and accelerated apoptosis compared with cells from miR-21 WT controls (Figures 3A and 3B; Movies S1 and S2). In cultured human carotid artery SMCs, miR-21 induction was able to suppress apoptosis, while miR-21 inhibition prompted phosphatase and tensin homolog (PTEN) and programmed cell death 4 (PDCD4) upregulation without further triggering the apoptotic intensity (Figures 3C and 3D). PTEN and PDCD4 are two well-known miR-21 targets, exerting cell survival functions upon miR-21 deregulation.[11] Efficiency of miR-21 modulation (inhibition and mimicry) was assessed in cultured human carotid artery SMCs (Figure S3A).

REST-miR-21 Feedback Loop Regulates SMC Fate

To investigate potential *in vivo* upstream and downstream regulators of miR-21, we performed a mouse transcriptomic array (MTA; complete dataset uploaded to Gene Expression Omnibus [GEO]) on samples from our inducible plaque rupture model. In comparison with contralateral, sham-operated controls, we discovered the RE1-silencing transcription factor (REST) as the most upregulated gene in unstable plaque tissue specimen (Figures 4A and 4B). In order to determine if REST could possibly be regulating miR-21, we analyzed possible miR-21/REST interactions by using the Ensembl Regulatory Elements (ENSR) *in silico* tool.[17,18] According to ENSR, the transcription factor REST is 1 of 223 genes with a predicted binding site in the promoter region of the miR-21 gene (primary-miR-21). Furthermore, among those genes, REST was the most significantly deregulated (induced) transcription factor in response to experimental plaque rupture (Figure 4B; complete list of all transcription factors with fold change and false discovery rate [FDR]-corrected p value in Table S1). Immunohistochemical analysis confirmed the upregulation of REST in ruptured atherosclerotic mouse plaques (Figure 4C). In addition, REST was dramatically upregulated in the *Apoe*$^{-/-}$*miR-21*-deficient mice in comparison with *Apoe*-deficient but *miR-21*-sufficient mice (Figure 4D). Therefore, we further investigated the possible interaction between miR-21 and REST.

In cultured human carotid artery SMCs, vector-based overexpression of REST was able to suppress proliferation while substantially stimulating the rate of apoptosis (Figure 4E). Consistent with previous reports that REST offers two binding sites in the miR-21 gene promoter region,[19,20] we observed inhibitory effects of induced REST on miR-21 expression (Figure 4F). In addition to previous findings, were we able to discover that miR-21 in turn can negatively regulate REST levels in human carotid artery SMCs (Figure 4G). miR-21 has a binding site in the 3′UTR of REST with a predicted binding free energy of −12.9 kcal/mol (Figure 4H). We performed a luciferase reporter assay to confirm miR-21 direct targeting of REST mRNA (Figure 4I). To test potential inducers of this REST-miR-21 axis, we stimulated SMCs with oxidized low-density lipoprotein (oxLDL) as well as tumor necrosis factor-α (TNFα). Interestingly, TNFα, but not oxLDL, increased REST expression in human SMCs (Figure 4J).

Finally, we were able to indicate that REST is, corresponding to lower levels of miR-21, more highly expressed in ruptured versus stable fibrous caps derived from human advanced atherosclerotic lesions on the mRNA level (Figure 4K) as well as the protein level (Figure 4L).

miR-21 Regulates Proliferation and Apoptosis in SMCs via the PTEN/AKT/ERK Signaling Pathway

Previous studies by others[21] and ourselves[11,12] have indicated that miR-21 induction can decrease expression of the PTEN tumor suppressor, leading to increased phosphorylation and activation of AKT, a master regulator of a pro-proliferative and anti-apoptotic phenotype in the vascular system. In the present study, we confirmed that miR-21 mimic treatment decreased PTEN levels in human carotid SMCs (Figures 5A–5D). Consistently, *Apoe*$^{-/-}$*miR-21*$^{-/-}$ mice exhibited significantly increased levels of PTEN and decreased phosphorylated AKT and ERK1/2 in aortic tissue specimen compared with littermate *Apoe*$^{-/-}$*miR-21*$^{+/+}$ controls (Figure 5E). In addition, *Apoe*$^{-/-}$*miR-21*$^{-/-}$ mice displayed higher PTEN expression in thinned fibrous caps of advanced atherosclerotic carotid artery plaques (Figure 5F).

miR-21 Deficiency Promotes Oxidized LDL Uptake in Peritoneal Macrophages via Activation of NF-kB Nuclear Translocation

Although no difference of plasma total cholesterol and triglyceride levels could be detected (Figure S2), *Apoe*$^{-/-}$*miR-21*$^{-/-}$ mice presented with an increase in lesion area in the aortic root and arch when reaching 16 weeks of age compared with significantly smaller lesions of *Apoe*$^{-/-}$*miR-21*$^{+/+}$ littermate controls fed a regular chow diet (Figures 6A–6C). The fact that the *Apoe*$^{-/-}$*miR-21*$^{+/+}$mice have very little lesion formation is consistent with previous studies, reporting foam cell formation (and not advanced lesions) in 15-week-old male *Apoe*$^{-/-}$ mice.[22] When staining for the macrophage marker Mac-2, we discovered enhanced accumulation of Mac-2-positive cells in plaques of *Apoe*$^{-/-}$*miR-21*$^{-/-}$ mice (Figure 6D). Thus, we evaluated the ability of peritoneal macrophages

in cultured HCtASMCs, while stimulating their apoptosis. REST knockdown using siRNA increases cell proliferation significantly. (F) Overexpression of REST leads to miR-21 reduction, while REST inhibition increases miR-21 levels in cultured human carotid artery SMCs. (G) miR-21 modulation using mimics and anti-miRs in cultured human carotid artery SMCs reversely regulates REST mRNA expression (n = 3 per group; the transfection experiments were repeated twice for E–G). (H) Predicted human-miR-21-5p binding site in the REST 3′UTR. (I) Luciferase reporter assay indicates REST as a direct target of mi-21-5p upon miR-21 mimic stimulation. (J) TNF-α increases REST expression levels in human carotid artery SMCs compared with control. Treatment with oxLDL has no significant effect. (K) REST mRNA expression significantly increased in ruptured versus stable atherosclerotic plaques from human patients with carotid artery disease. (L) Immunohistochemical-based staining for REST indicates elevated levels in ruptured versus stable human carotid artery plaques. *p < 0.05 versus NC or SCR or stable. Mean ± SEM. Bar, 100 μm. Data in (E) were analyzed using two-way repeated-measures ANOVA; all other data were compared using Student's t test.

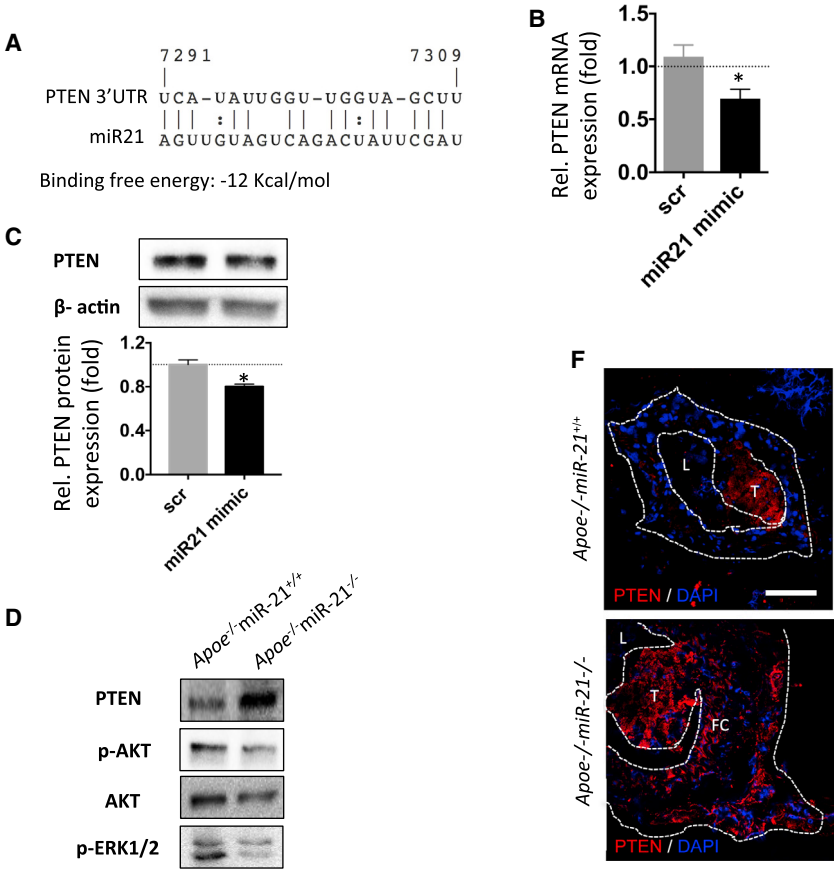

Figure 5. miR-21 Targets PTEN/AKT/ERK Signaling in SMCs

(A) Human-miR-21-5p non-canonical binding site in the PTEN 3′UTR. (B–D) Significant PTEN mRNA (B) and protein reduction (C and D) after miR-21 mimic versus scramble treatment in human carotid artery SMCs. (E) Western immunoblotting confirms significantly increased levels of PTEN and decreased phosphorylated AKT and ERK1/2 in aortic tissue specimen of *Apoe*$^{-/-}$*miR-21*$^{-/-}$ mice compared with those from their *Apoe*$^{-/-}$ *miR-21*$^{+/+}$ littermate controls (n = 3 per group). (F) *Apoe*$^{-/-}$*miR-21*$^{-/-}$ mice display higher PTEN expression in fibrous caps of advanced atherosclerotic plaques and carotid arteries upon PTEN immunofluorescent staining. FC, fibrous cap; L, lumen; T, thrombus. *p < 0.05 versus SCR. Mean ± SEM. Bar, 100 μm. Groups were compared using Student's t test.

from both mouse strains to transform into foam cells by studying their behavior upon oxidized LDL (oxLDL) stimulation. Using fluorescently labeled oxLDL particles, we detected an increase in oxLDL uptake of macrophages derived from *Apoe*$^{-/-}$*miR-21*$^{-/-}$ mice, which could be attenuated by using pretreatment with an NF-kB translocation inhibitor (Figures 6E and 6F; Movie S1B). Consistently, we observed an enhanced NF-kB nuclear translocation in *Apoe*$^{-/-}$*miR-21*$^{-/-}$ macrophages, which could be rescued by NF-kB translocation inhibitor pretreatment (Figure S4), indicating and confirming[23] that miR-21 regulates NF-kB activity and thus is affecting foam cell formation and lipid core development during atherogenesis (Figures 6G and 6H). Moreover, were we able to detect that supernatant, derived from cultured macrophages of *Apoe*$^{-/-}$*miR-21*$^{-/-}$ mice, were able to suppress the proliferation of mouse aortic SMCs, with or without oxLDL stimulation (Figure 6I).

Locally Enhanced Delivery of miR-21 Mimics Prevent Advanced Mouse Plaques from Rupture

With the aim of testing optimized tools of locally delivering miRNA modulators, we decided to use ultrasound-targeted microbubble destruction (UTMD) to distribute miR-21 mimics into advanced lesions prone to rupture (Figure 7A). First, we confirmed efficient local absorption of *Fas-red*-labeled miRNA scrambled control oligonucleotides into right injured common carotid arteries after performing the inducible plaque rupture model. The contralateral left side served as an internal control without ultrasound stimulation (Figure 7B). Next, we tested enhanced local miR-21 mimic delivery in *Apoe*$^{-/-}$*miR-21*$^{+/+}$ and *Apoe*$^{-/-}$*miR-21*$^{-/-}$ mice. In both groups, miR-21 mimicry rescued the plaque phenotype, displaying fewer signs of ruptured lesions, mainly through enhanced SMC proliferation and consequentially thicker fibrous cap structures, as indicated by the number of SMA-positive cells. A sufficient increase of miR-21 levels, as well as reduction of PTEN and REST as its target genes, could be detected in the targeted carotid artery (Figures 7C–7E, S3B, and S5), while hepatic and brain miR-21 expression remained unchanged compared with scrambled control miRNAs when applying the UTMD method (Figures 7F and S3C). Systemic forms of injection without ultrasonographically induced microbubble burst led to increased miR-21 levels in the liver compared with the scrambled miRNA control group (Figure 7F).

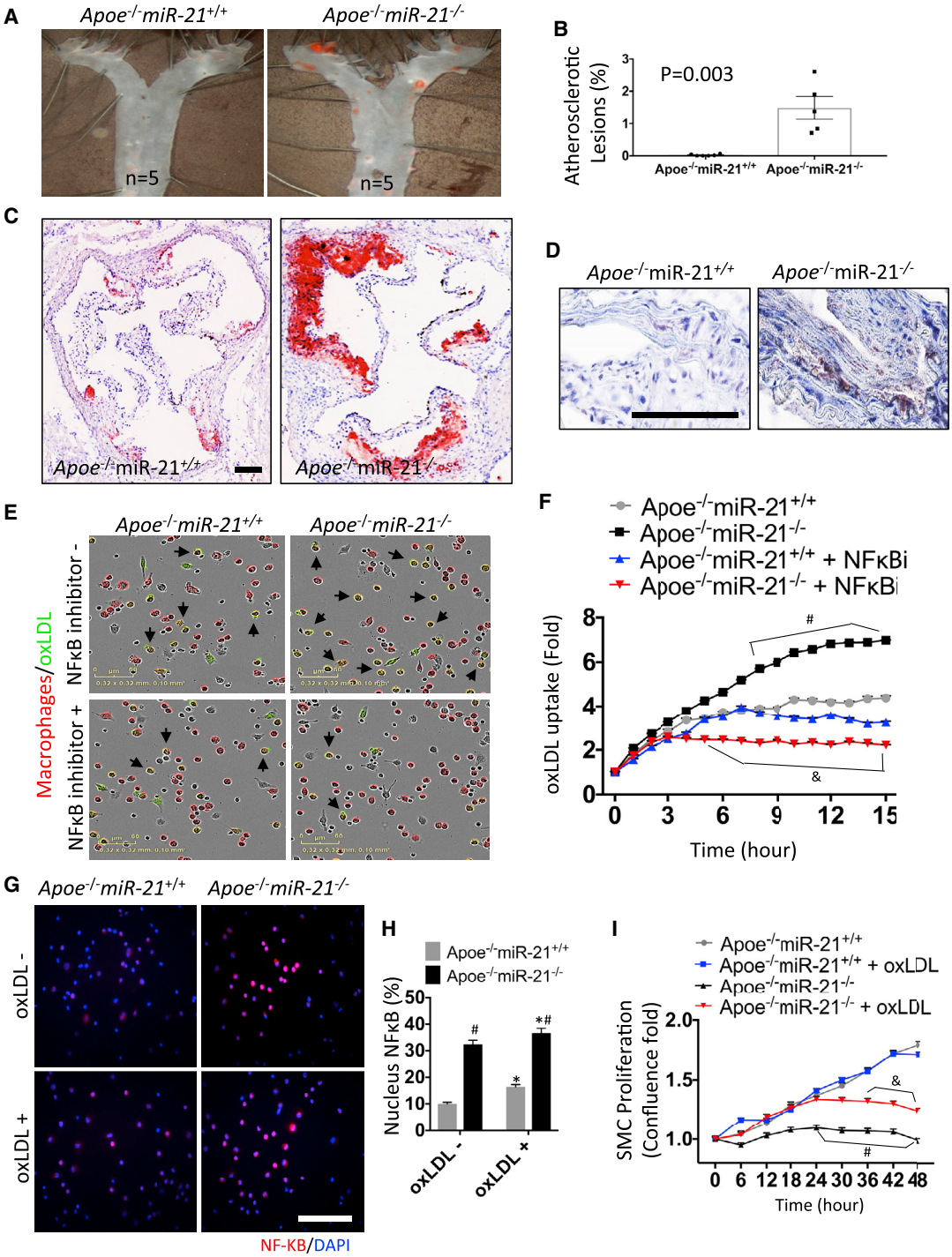

Figure 6. miR-21 Deficiency Activates NF-kB Nuclear Translocation and Enhances OxLDL Uptake in Mouse Peritoneal Macrophages

(A and B) Atherosclerotic lesions were assessed by staining with Sudan IV (A) and expressed as percentage surface area for the entire aorta as well as individual segments (B). Data are given as mean ± SEM (n = 5; *p = 0.03 versus the Apoe$^{-/-}$miR-21$^{+/+}$ mice). (C) Substantially larger atherosclerotic lesions could be detected in aortic roots of Apoe$^{-/-}$miR-21$^{-/-}$ mice assessed with oil red O staining. (D) Increased macrophage deposition and activity (Mac-2-positive cells) in carotid artery atherosclerotic plaques of Apoe$^{-/-}$miR-21$^{-/-}$ mice. (E) Greatly enhanced FITC-conjugated oxLDL (green) uptake of peritoneal macrophages (Alexa Fluor 647 labeled red) of Apoe$^{-/-}$miR-21$^{-/-}$ mice (n = 7), compared with Apoe$^{-/-}$miR-21$^{+/+}$-derived macrophages (n = 8), which could be effectively blocked via pretreatment with a NF-kB translocation inhibitor (indicated with arrows; Apoe$^{-/-}$miR-21$^{-/-}$, n = 5; Apoe$^{-/-}$miR-21$^{+/+}$, n = 3) being assessed kinetically with live-cell imaging (F). (G) Fluorescent staining with anti NF-kB p65, to

(legend continued on next page)

DISCUSSION

miR-21 has previously been indicated as an important mediator in cardiovascular diseases, such as cardiac fibrosis and heart failure,[24,25] abdominal aortic aneurysm development and expansion,[11] and atherogenesis.[26–28] A very recent report by Canfrán-Duque et al.[29] has further elucidated that the absence of miR-21 in macrophages results in an accelerated progression of atherosclerosis, intra-plaque necrosis, and overall vascular inflammation. The authors described an intriguing mechanism that involves upregulation of the miR-21 target MKK3, which triggers p38-CHOP and JNK signaling. Limited macrophage survival in their setting accelerated macrophage death, while inducing the post-transcriptional degradation of the cholesterol transporter gene ABCG1.

In addition to the study by Canfrán-Duque et al.,[29] our present study expands upon their observations by showing the relevance of miR-21 in fibrous caps of human advanced lesions, in which apart from its role in macrophages, we were able to unravel a second important mechanism through which miR-21 augmentation destabilizes atherosclerotic plaques. Depletion of miR-21 limited SMC proliferation rates and enhanced apoptosis, leading to impaired vascular remodeling upon ligation injury and fibrous cap thinning in our inducible plaque rupture model. Our observations *in vivo* were further confirmed *in vitro* by using dynamic live-cell imaging of human and mouse arterial SMCs.

Mechanistically, we identified a novel upstream repressor of miR-21 expression in vascular disease, which interestingly gets tempered itself via a feedback loop by being a direct target of miR-21. The transcription factor REST, previously also known as neuron-restrictive silencer factor (NRSF), a reported upstream repressor of miR-21 during neuronal development,[20,30,31] increased in both human unstable atherosclerotic lesions and upon inducing plaque rupture experimentally in mice. Previous reports on REST have identified this gene as a transcriptional repressor of neuronal genes in non-neuronal tissues.[20] The protein is furthermore found in undifferentiated neuronal cells, in which REST is thought to act as a master negative regulator of neurogenesis.[30] Its contribution to vascular disease development and SMC dynamics was previously unknown. Here, REST exerts an inhibitory role on proliferating SMCs, while enhancing their apoptosis. Similar feedback mechanisms such as miR-21:REST are not new for miRNAs and have been described in stress signaling and human disease early on.[32]

TNF-α, a well-established regulator of inflammation and aggravation of atherosclerosis, can stimulate REST expression,[33] which limits miR-21 levels downstream. miR-21 itself regulates SMC fate decisions through the PTEN/AKT/ERK signaling pathways. Targeting PTEN, among other apoptosis-mediating genes, such as PDCD4 and BCL-2, has already been validated for miR-21.[34–36]

Apart from miR-21's contribution to fibrous cap stability by regulating SMC survival and rupture-limiting proliferation, we observed accelerated lesion formation and progression, presumably unrelated to SMC dynamics. *Apoe*$^{-/-}$*miR-21*$^{-/-}$ mice displayed enlarged plaques in the aortic root and arch, already at age 16 weeks on a regular chow diet. This finding is consistent with those of previous studies focusing on the role of macrophages in *Ldlr*$^{-/-}$*miR-21*$^{-/-}$ and miR-21-depleted mice.[26,29] Those studies revealed a pro-atherosclerotic and pro-inflammatory mechanism through which loss of miR-21 drastically aggravates the critical advancement of atherosclerosis and unstable lesions.

In addition to previous studies, we were able to discover *ex vivo* that peritoneal macrophages from double-knockout mice represent a significantly enhanced uptake of oxLDL particles. The increase in uptake triggers the formation of foam cells and lipid accumulation within lesions, leading to an acceleration of inflammatory signaling to neighboring cells. Indeed, we were able to see that SMCs being treated with the supernatant of *Apoe*$^{-/-}$*miR-21*$^{-/-}$ macrophages display substantially limited proliferation rates. This intercellular crosstalk likely plays a very important role in limiting fibrous cap stability and negatively affects plaque progression. In addition to the aforementioned study by Canfrán-Duque et al.,[29] we evaluated the regulatory role of miR-21 in, and through, the NF-kB signaling pathway.[37,38] One report described the direct contribution of NF-kB translocation in human aortic endothelial cells.[39] In our study, an enhancement in NF-kB p65 nuclear translocation was detected in macrophages of *Apoe*$^{-/-}$*miR-21*$^{-/-}$ mice, even before oxLDL stimulation was performed. This indicates a more inflammatory state for macrophages in miR-21-deficient mice. Consistently, pretreatment with a NF-kB translocation inhibitor significantly reversed the augmented oxLDL uptake from macrophages being derived from *Apoe*$^{-/-}$*miR-21*$^{-/-}$ mice.

miRNA-based therapeutics are at the doorstep of entering the clinic, providing an exciting new arsenal of powerful targets to tackle the burden of various diseases.[40] It remains more challenging to overexpress a miRNA to induce gain of function using mimics than to inhibit them with antisense oligonucleotides in their various formulations.[41] Several preclinical and clinical studies have shown unprecedented disease-limiting effects of miRNA inhibitors, also known as anti-miRs, including studies from the field of atherosclerosis and cardiovascular disease.[42]

determine localization (nuclear) in macrophages with or without oxLDL stimulation. (H) Quantification indicates increased levels of NF-kB nuclear translocation of Apoe$^{-/-}$miR-21$^{-/-}$ mice macrophages before oxLDL stimulation, which becomes further enhanced upon stimulation with oxLDL (n = 4). (I) Supernatant of cultured peritoneal macrophages in triplicates derived from Apoe$^{-/-}$miR-21$^{-/-}$ mice (pooled supernatant from two mice) display suppressing effects on primary mouse aortic SMC proliferation rates compared with those originating from Apoe$^{-/-}$miR-21$^{+/+}$ mice (pooled supernatant from two mice) and live-cell imaging experiments were repeated twice. *$p < 0.05$ versus oxLDL, #$p < 0.05$ versus Apoe$^{-/-}$miR-21$^{+/+}$, &$p < 0.05$ versus Apoe$^{-/-}$miR-21$^{-/-}$. Mean ± SEM. Bar, 100 μm. Data presented in (F) and (I) were analyzed using two-way repeated-measures ANOVA; all other data were compared using Student's t test.

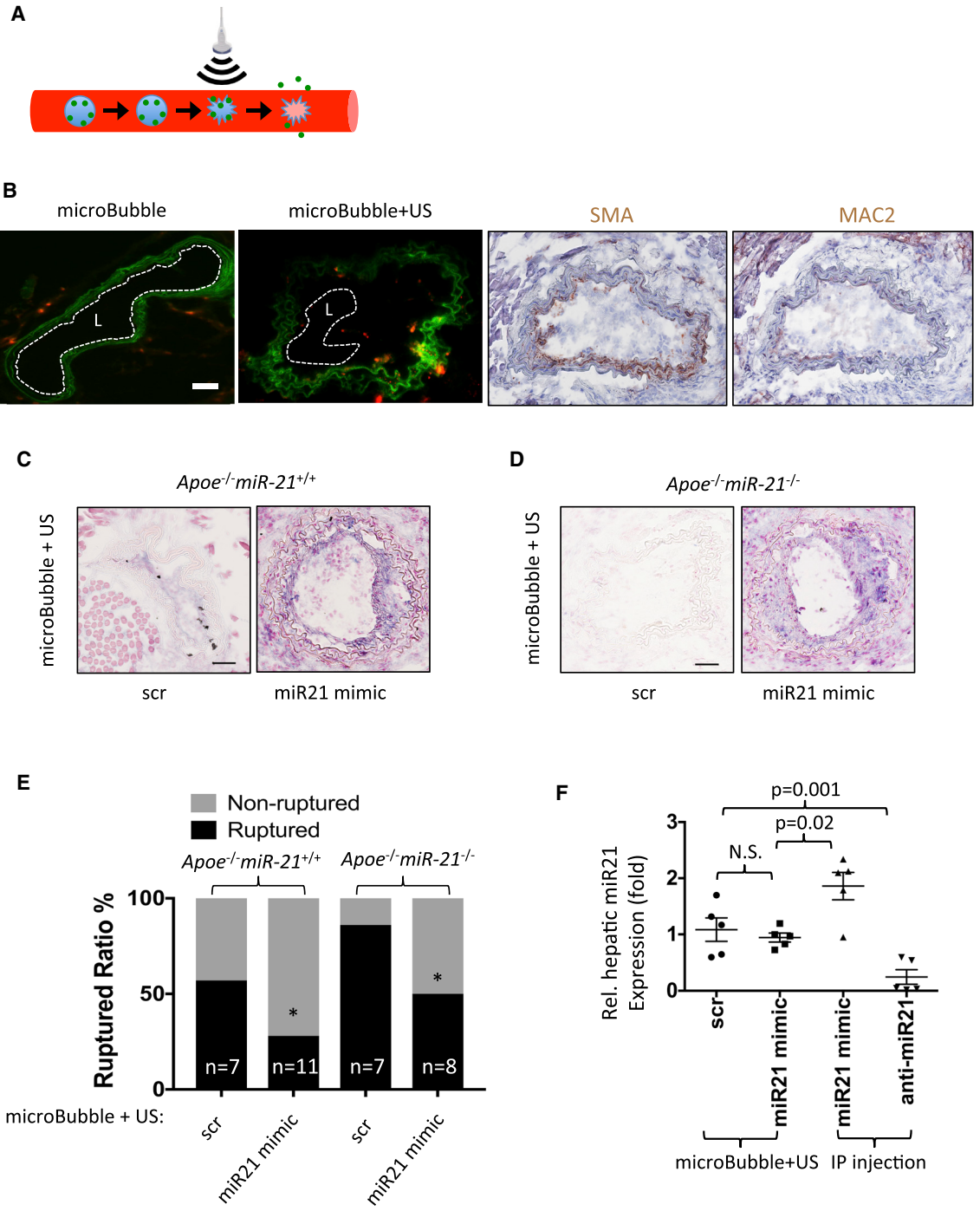

Figure 7. Local miR-21 Induction Enhances Atherosclerotic Fibrous Cap Stability without Off-Target Effects

(A) Descriptive cartoon on how to apply *in vivo* ultrasound-targeted microbubble destruction (UTMD)-induced local delivery of miRNA mimic or scramble control oligonucleotides at 1 MHz. The transducer is placed on the right carotid artery for 15 min, allowing the miR-21 mimic or scrambled control to be released upon microbubble burst into vascular tissue. (B) Fluorescent microscopy and immunohistochemical analysis of cryo-sections of mouse carotid arteries indicating uptake of the scrambled-controls (red) into media and plaque tissue and elastin fibers (green). Images are representative images for several experimental mice per group (n = 6). MB, microbubble; US, ultrasound. (C and D) ISH of carotid plaques show enhanced miR-21 deposition in plaques being treated with miR-21 mimic in both Apoe$^{-/-}$miR-21$^{+/+}$(C) and

(legend continued on next page)

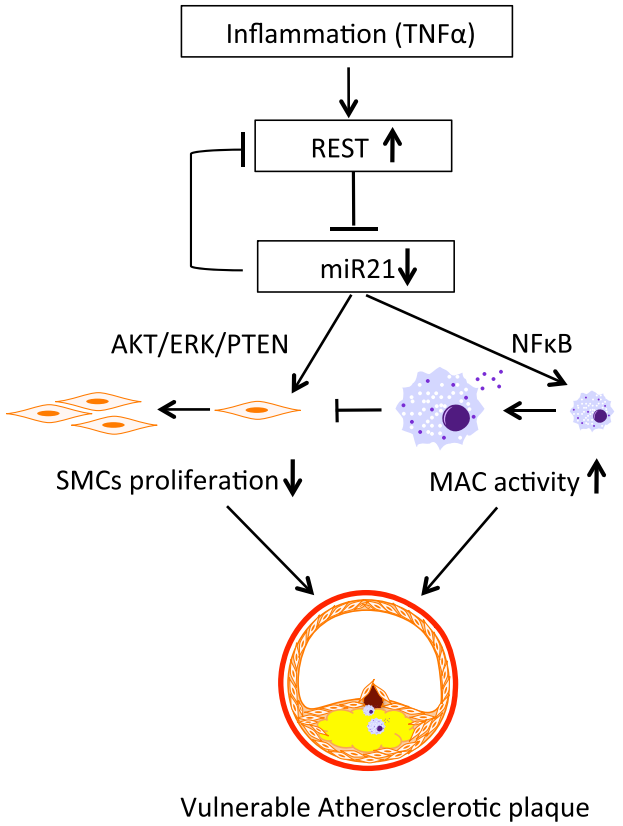

Figure 8. Proposed Mechanism of Action for miR-21 in Advanced Atherosclerosis

miR-21 regulates SMC proliferation and apoptosis, as well as foam cell formation upon induction through the transcription factor REST. miR-21 signals downstream through the PTEN/AKT/ERK signaling cascade, mainly in SMCs, while macrophage activity is dependent on miR-21 NF-kB crosstalk. Activated macrophages can limit the proliferation rate of SMCs. Taken together the described mechanisms lead to advanced atherosclerotic lesions with thinned fibrous caps and vulnerable plaques.

One limitation in particular for the cardiovascular field is reported off-target effects in organ systems, in which systemically injected miRNA modulators accumulate to a much higher extent than the targeted heart or vessel wall.[43] In our case, increased levels of miR-21 are well known to induce cardiac[25] and renal fibrosis.[44,45] Furthermore, miR-21 has been recognized to exert oncogene-like functionality, and systemic stimulation of its expression appears unattractive for translational purposes, as tumor progression might get triggered in organs in which miR-21 has been reported for being engaged in cancer development, such as in the lung, liver, kidney, and pancreas.[46–49] We have previously successfully used drug-eluting stents to locally deliver an anti-miR targeting miR-21 to limit the development of in-stent restenosis.[12] In the present study, we attempted ultrasound-guided microbubble burst to avoid undesired off-target effects of miRNA modulation.

Nanoparticles as scavengers for delivery of therapeutic agents, in particular nucleic acids, have drawn great attention in recent years, for both imaging purposes and therapeutic applications.[50] UTMD has proved to be an effective delivery method for miRNA mimics, as well as other gene-targeting strategies in experimental *in vivo* studies.[51–54] Our present results indicate successful use of UTMD-enhanced delivery of miR-21 mimics into the carotid artery to rescue vulnerable plaques, while not exerting off-target effects in the liver, the prototypical organ in which antisense oligonucleotides are known to assimilate. Future studies should test if the delivery strategy of UTMD-enhanced miR-21 modulation could be applied not only in carotid arteries but also in the coronary system, as well as other advanced atherosclerotic lesion sites prone to rupture.

In conclusion, our present study expands the role of miR-21 in the cardiovascular system to a key function in regulating fibrous cap stability of advanced atherosclerotic lesions via inducing proliferation rates and blocking apoptosis of SMCs in human and mouse carotid arteries (Figure 8). Local rescue of miR-21 expression in vulnerable plaques may become a promising future therapeutic approach with relevance for clinical applications.

MATERIALS AND METHODS

Laser Capture Micro-dissection of Advanced Atherosclerotic Carotid Artery Plaques

Atherosclerotic lesions, stable and ruptured (vulnerable), were paraffin-embedded, sectioned, and stained with H&E on RNase-free glass slides, using a standardized protocol briefly described below. Sections were pre-treated with UV light at 254 nm for 30 min to overcome the hydrophobic nature of the membranes and to enhance adhesion of the paraffin-embedded sections. Between five and ten consecutive slides per individual patient were micro-dissected and then pooled for miRNA expression analysis. In preparation for laser pressure catapulting, sections were first de-paraffinized with xylene (2 × 2 min) and decreasing ethanol concentrations (100%, 96%, and 70% each for 1 min). Sections were then rinsed in RNase-free water and stained for 10 min with Mayer's hematoxylin (Sigma-Aldrich), again rinsed for 3 min in RNase-free water, and then consecutively stained for 3 min with eosin (Sigma-Aldrich). Finally, samples were dehydrated with increasing ethanol concentrations, before briefly being air-dried at room temperature. After microdissection and catapulting, the fibrous cap sample (for an example, see Figure 1A) was collected into AdhesiveCaps (Zeiss), and 350 μL of RLT buffer (QIAGEN) was added and mixed by inversion after closure.

Apoe$^{-/-}$miR-21$^{-/-}$(D) groups upon local delivery of microbubble-carrying miR-21 mimic versus scrambled controls after ultrasound stimulation. (E) miR-21 local delivery induces a significant reduction of the plaque rupture rate compared with scrambled-control treated mice. Data were analyzed using chi-square or Fisher's exact test. (F) Compared with systemic intraperitoneal (IP) injection of miR-21 mimics, no significant increase of miR-21 levels in hepatic tissue from mice upon local delivery with UTMD versus scrambled-control injected mice can be detected. Groups were compared using Student's t test. Data are given as mean ± SEM. Bar, 50 μm.

The lysate was centrifuged for 5 min at 13,000 rpm and stored at −80°C. RNA extraction from catapulted, micro-dissected samples was performed using the RNeasy Micro Kit (QIAGEN) following the manufacturer's protocol. RNA was quantified by Nanodrop (Agilent Technologies) and RNA quality verified using an Agilent 2100 Bioanalyzer (Agilent Technologies). Samples required 260/280 ratios > 1.8 and sample RNA integrity numbers > 7 for inclusion. The Taqman High Capacity cDNA Transcription Kit (Thermo Fisher Scientific) was used for cDNA synthesis, and primer assays for miRNAs and 18S (endogenous control; both from Thermo Fisher Scientific) were used to detect changes in expression levels.

In Situ Hybridization

In situ hybridization (ISH) of miR-21 was performed according to manufacturer's protocol "miRCURY LNATM miRNA ISH Oprimization Kit" (Exiqon, instruction manual version 3.0, January 2016) with modification for fresh frozen sections (Exiqon, supplementary guidelines version 1.1) as described previously.[11] The sequence of the LNA miR-21 detection probe was /SDigNfrCAACATCAGT CTGA T AAGCTN3Dig_N/. The LNA control scrambled (SCR)-miR sequence was /5DigN/GTGT AACACGTCTATACGCCCA/ 3Dig_N/.

In Vitro Cell Culture and miRNA Modulation

Human carotid artery SMCs (HCtASMCs; Cell Applications) of passage 5–8 were seeded at 100,000 cells/well (in a 6-well plate) or 5,000 cells/well (in a 96-well plate); after cells reached 70%–80% confluence, growth medium was replaced with Opti-MEM (GIBCO, Thermo Fisher Scientific) serum-free medium supplemented with 0.4% fetal bovine serum (FBS; GIBCO). Anti-miR-21, pre-miR-21, miR-21 mimic, and mismatch (scrambled) control oligonucleotides (GIBCO, Thermo Fisher Scientific) were diluted in Opti-MEM and applied at 50 nM using Lipofectamine RNAiMAX Transfection Agent (GIBCO, Thermo Fisher Scientific), according to the instructions of the manufacturer. For REST modulation, we used REST plasmid (25 ng/well, #RC211570; Origene) and small interfering RNA (siRNA) (25 nM, s11934; Thermo Fisher Scientific). Cells were harvested for gene expression assay 24–48 hr after miR-21 or REST modulation using TaqMan assay system according to the manufacturer's instructions (Thermo Fisher Scientific).

Knockout Mouse Models

miR-21-deficient mice on a C57BL/6J background[55] were kindly provided by Dr. Maja Jagodic (Karolinska Institute). The genotype was determined by PCR, using primers for miR-21 (common: AAGG GCTCCAAGTCTCACAAGACA; WT: TTGCTTTAAACCCTGCC TGAG CAC; mutation: ACTTCCATTTGTCACGTCCTGCAC). In order to generate mice suitable for studies on atherosclerosis and to use the plaque rupture model, we crossbred *miR-21*$^{-/-}$ mice with apolipoprotein-E-deficient mice (Taconic Biosciences) to generate Apoe$^{-/-}$*miR-21*$^{-/-}$ double-knockout mice and *Apoe*$^{-/-}$ *miR-21*$^{+/+}$ littermates. This study was carried out in accordance with the recommendations in the Guide for the Care and Use of Laboratory Animals of the Swedish Board of Agriculture. The protocol was approved by the Committee on Ethics of Animal Experiments of Northern Stockholm (permit number N48/16). All cages were environmentally enriched with paper wool, mice were fed a normal rodent chow, and water was provided *ad libitum* with a 12-hr light/dark cycle.

Mouse Primary Aortic SMC Culture

SMCs from aortas originating from 6- to 8-week-old mice were isolated as published previously by others.[56] In brief, three aortas from the same genotype were pooled. Cells isolated from *Apoe*$^{-/-}$*miR-21*$^{-/-}$ or *Apoe*$^{-/-}$ *miR-21*$^{+/+}$ mice were passaged three times before undergoing further studies. Cells were allowed to grow to ∼70% confluence in DF10 (DMEM-F12 medium [GIBCO] containing 10% FBS [GIBCO] and 100 U/mL penicillin/streptomycin [GIBCO]).

Vascular SMC Proliferation and Apoptosis Analysis Using Live-Cell Imaging

HCtASMC and mouse aortic SMCs were plated at 40%–50% confluence in 24-well plates. Cells were starved for 8 hr in DMEM-F12 (Thermo Fischer Scientific), then supplemented with either 2% or 5% FBS. Cells were transfected with anti-miR-21, miR-21 mimic, and mismatch (scrambled) control oligonucleotides as described above, or REST plasmid and siRNA as well as negative controls, and then analyzed using the IncuCyte Live Cell ZOOM Imaging System for up to 72 hr. Proliferation was measured as percentage of confluence. For apoptosis, the IncuCyte Kinetic Caspase-3/7 Apoptosis Assay Reagent (Essen BioScience) was used according to the manufacturer's protocol.

Carotid Ligation Model

At 12 weeks of age in male WT and miR-21 knockout mice, the right carotid artery was ligated at the bifurcation with 8-0 sutures as previously described.[57] The animals were anesthetized using isoflurane/O_2 (2:1). Subcutaneous injection of buprenorphine (0.1 mg/kg) was applied before and after surgery for pain relief. Twenty-eight days after ligation, the mice were sacrificed, and the carotid arteries were embedded in OCT compound and fresh-frozen before further immunohistochemistry preparation and morphometric analysis.

Inducible Carotid Artery Plaque Rupture Model

To investigate atherosclerotic plaque development and rupture, 12-week-old male *Apoe*$^{-/-}$ *miR-21*$^{-/-}$ double-knockout mice and *Apoe*$^{-/-}$*miR-21*$^{+/+}$ littermates were used. We used an inducible plaque rupture model modified of the carotid ligation/cast approach described by others as well as ourselves.[16,58–60] Briefly, mice received an incomplete ligation (Vicryl 5-0 suture; Ethicon Endo-Surgery) of the common right carotid artery (proximal to bifurcation) for 4 weeks, triggering intimal hyperplasia and stable carotid atherosclerotic lesion development. Then, to provoke rupture of the developed plaque, a conical polyethylene cuff with diameters of 300 and 150 μm (Promolding) was placed proximal to the ligation site for 4 days to induce fibrous cap collagen degradation. All animals were anesthetized using isoflurane/O_2 (2:1). Subcutaneous injection of buprenorphine (0.1 mg/kg) was applied before and after surgery for pain relief for both ligation and cuff placement. Approximately 50%–60% of the

16-week-old *Apoe*$^{-/-}$ male mice display features of ruptured plaques, such as endothelial cracks, ulcerations, intra-luminal thrombus formation, and intra-plaque hemorrhages.[61,62]

In Vivo miR-21 Local Carotid Modulation by UTMD

Mice first underwent the mouse carotid rupture model and in addition received an intravenous bolus of 200 μL cationic microbubbles (2×10^9 cMB/mL in H_2O; SonoVue). The microbubbles were charge-coupled with miR-21 mimic or FAM-labeled scrambled miRNA control oligonucleotides (all from GIBCO, Thermo Fisher Scientific). After the first treatment at baseline, microbubble injections were repeated 10, 20, and 27 days after ligation of the right common carotid artery. For UTMD, ultrasound was transmitted over the targeted carotid artery using a phased transducer (Sonitron GTS Sonoporation System) for 15 min with 1 MHz, 2.0 w/cm^2, and 50% duty cycles as previously described.[51,63] The location below the ligated area was determined by using a Vevo770 ultrasound imaging system. In order to visualize the localization of the FAM-labeled control oligonucleotides, carotids were dissected and placed into optimal cutting temperature (OCT) Cryomount compound (Histolab), snap-frozen, and stored at −80°C. Six-micrometer-thick sections were washed three times in PBS and sealed with Vectashield mounting medium (Vector Laboratories). FAM-labeled oligonucleotides were observed by using a fluorescent microscope (Zeiss).

In Vivo miR-21 Systemic Modulation

For inhibition of miR-21, we used 10 mg/kg LNA-carried anti-miR-21 (Exiqon) diluted in 200 μL PBS. Mice (n = 6) were injected intraperitoneally on the day they underwent carotid ligation (day 0) and day 20 after ligation.

For miR-21 systemic overexpression, we used 2 mg/kg miR-21 mimic (Ambion; Thermo Fisher Scientific), using Jet-PEI (Polyplus-transfection) as the delivery vector. Mimics were injected intraperitoneally (at the time of carotid ligation and then 10, 20, and 28 days after the cuff was placed; n = 6).

Mouse Tissue and Blood Collection

Mouse tissue was harvested according to standard procedures. Mice were euthanized through CO_2 inhalation. Blood was collected by heart puncture and placed into EDTA-coated tubes and centrifuged for 10 min at 10,000 rpm, and collected plasma was snap-frozen. Animals were perfused with cold 0.9% NaCl. For RNA analysis, right carotid arteries were divided into "ruptured" and "non-ruptured" according to the macroscopic presence or absence, respectively, of thrombus in the cast area, which is later confirmed with immunohistochemistry (IHC) staining (α-smooth muscle actin and fibrin). Per outcome (ruptured/non-ruptured), two samples were pooled to obtain enough total RNA for analysis. For miR-21 expression analysis after miR-21 mimic local delivery or intraperitoneally injection, right-side carotid arteries were harvested. Tissue was stored in RNAlater (Invitrogen, Thermo Fisher Scientific) and stored at −20°C until further processing. RNA samples were extracted using the RNeasy Micro Kit (QIAGEN). RNA was quantified with NanoDrop (Agilent Technologies), and RNA and miRNA quality was verified using the Agilent 2100 Bioanalyzer (Agilent Technologies). For tissue histology and oligonucleotide tracking, both carotid arteries were harvested and embedded in OCT, snap-frozen, and stored at −80°C.

Mouse Transcriptome Array and Data Analysis

For the mouse transcriptome analysis, the right common carotid arteries of a total of 18 male *Apoe*-deficient mice after ligation and cuff placement were harvested and stored in RNAlater. Eleven non-ligated left arteries were used as controls. RNA mouse transcriptome array (MTA; Affymetrix 902514) and differential expression analysis (Affymetrix transcriptome analysis console version 3.0) was performed according to the manufacturer's instructions. In this study, the dataset was queried for values of a select number of transcripts. Results are given as relative mRNA expression in a.u. $\log_2$-transformed fold changes, compared with background intensity.

oxLDL Stimulation and Uptake by Peritoneal Macrophages

Lipoproteins used for foam cell formation and oxLDL uptake were isolated from human plasma obtained from the Blood Central at Karolinska University Hospital through sequential ultracentrifugation. Briefly, plasma was ultracentrifuged for >22 hr at 40,000 rpm and 4°C. The uppermost phase containing chylomicrons was discarded, and the intermediate phase containing LDL and high-density lipoprotein (HDL) was collected. The density of the LDL/HDL phase was adjusted to 1.063 g/mL with potassium bromide (Sigma-Aldrich) and ultracentrifuged as previously described. The upper phase containing LDL was collected and desalted using a PD-10 column (GE Healthcare). LDL was oxidized overnight at 37°C using 20 μM copper sulfate ($CuSO_4$; Merck), and the reaction was stopped using 1 mM EDTA (Sigma-Aldrich). oxLDL was conjugated to fluorescein isothiocyanate (FITC) by incubating oxLDL with 50 μg FITC/mg oxLDL overnight at 4°C. Excess FITC was removed using a PD-10 column. Mice were sacrificed with CO_2 and injected intraperitoneally with 8 mL PBS, and extracted cells were washed and re-suspended in RPMI media containing penicillin and streptomycin and 2% fetal calf serum (GIBCO). Cells (4.5×10^5) were plated into a 48-well cell culture plate and allowed to adhere for 2 hr at 37°C and 5% CO_2. Cells were washed twice with PBS and incubated with anti-CD11b (Clone M1/70) conjugated with Alexa Fluor 647 at 2.5 μg/mL for 15 min at 37°C and 5% CO_2. Cells were again washed and loaded with 20 μg/mL of FITC conjugated oxLDL (prepared in house as described) and placed into IncuCyte ZOOM (Essen BioScience) for 24 hr with hourly scans using a 20× objective. To investigate the mechanism, 9 μM NF-kB nucleus translocation inhibitor SN50 (Merck) was added to cultured macrophages before oxLDL loading.

Tissue Histology and IHC and Immunofluorescent Analysis

Mouse OCT-embedded frozen carotid artery tissue was cut into 6-μm-thick sections, dried, and stored at −80°C. Human carotid arterial plaque material was fixed for 24 hr in 4% paraformaldehyde at room temperature, paraffin-embedded, and cut into 10-μm-thick sections. Control arteries (carotid, radial, iliac, or mammary) were obtained from deceased organ donors without any reported history

of cardiovascular disease. H&E staining was used for basic tissue morphology. Lipids were stained with oil red O (Sigma-Aldrich). Sections were stained with antibodies against SMA (ab5694), Ki-67 (ab16667), REST (ab202962), Mac-2 (ab53082), and PTEN (ab31392), all from Abcam, with secondary antibody, HRP goat anti-rabbit IgG (Vector Laboratories) or Alexa Fluor 488/546 goat anti-rabbit/mouse IgG for immunofluorescent analysis. *In situ* apoptosis detection of mouse carotid arteries cells was performed using the Click-iT Plus TUNEL assay kit (C10617; Invitrogen, Thermo Fisher Scientific). All histological analyses were obtained using NanoZoomer 2.0-HT Digital Slide Scanner (Hamamatsu Photonics). Fluorescent images were obtained using a fluorescence microscope (Zeiss) and analyzed by Zeiss Imaging Software.

In Vitro Immunofluorescent Analysis

The method for *in vitro* immunofluorescent analysis of PTEN and NF-kB nucleus translocation is described in detail in Supplementary Materials and Methods.

En Face Staining of Mouse Thoracic Aorta

The descending aorta was dissected and placed in 4% paraformaldehyde. The aorta was then pinned onto a paraffin bed with insect pins (AgnoTho's) and stained with Sudan IV. Images were captured using a DC480 camera connected to a MZ6 stereomicroscope (both from Leica). The additive area of all the plaques in a given aortic arch was calculated as a percentage of the total surface area of the arch. Quantitation of plaques was performed using ImageJ software (NIH).

Mouse Plasma Cholesterol and Triglyceride Measurements

Triglycerides were measured using Randox reagents; cholesterol was measured using a colorimetric Cholesterol Assay Kit (Abcam) following the manufacturer's protocols.

Real-Time qPCR

Total RNA from ligated and non-ligated carotid arteries or cultured cells was isolated using QIAGEN's miReasy Micro or Mini Kit. Relative gene and miRNA expression was assessed using TaqMan assays: human mi21 (#000397), humanU6 (#001973), human REST (Hs00958503_m1), human RPLPO (Hs99999902_m1), human PTEN (Hs02621230_s1), human SOX-2 (Hs01053049_s1), mouse miR-21 (#000397), mouse snoRNA202 (#001232), mouse REST (Mm00803268_m1), and mouse PTEN (Mm00477208_m1), all from Thermo Fisher Scientific.

Protein Isolation and Western Blotting

Mice aortas were homogenized in RIPA buffer cocktail (Thermo Fisher Scientific) including protease and phosphatase inhibitor cocktails (Sigma-Aldrich). Protein concentrations were determined using the bicinchoninic acid assay (Thermo Fisher Scientific) following the manufacturer's protocol. Protein samples (15 μg/well) were loaded on 4%–12% Tris-glycine gels (Thermo Fisher Scientific). Following electrophoresis and electrotransfer, the polyvinylidene difluoride (PVDF) membrane (Bio-Rad) was blocked with 5% milk-TBST (Bio-Rad) before primary antibody incubation. Western blot was performed with anti-mouse PTEN (154812, Abcam; 1:1,000), total (4695S, Cell Signaling; 1:3,000), and phosphorylated (4370, Cell Signaling; 1:1,000) ERK1/2, total (126811, Abcam; 1:2,000) and phosphorylated AKT antibodies (81283, Abcam; 1:2,000). β actin (A1978, dilution 1:8,000; Sigma-Aldrich) was applied as control. Densitometric quantification was carried out using ImageJ64 software. Western blot was performed with n = 3 $Apoe^{-/-}miR\text{-}21^{+/+}$ and $Apoe^{-/-}miR\text{-}21^{-/-}$ mice.

Statistical Methods

SPSS Statistics version 22 (IBM) was used to analyze the human patient data. To compare two groups, an independent-samples t test was used. Paired data were analyzed using a paired-samples t test. Differences between two or more groups and a control group were analyzed using one-way ANOVA plus Bonferroni correction for multiple comparison. Significant differences as percentages of plaque rupture were analyzed using chi-square testing. Non-parametric data were analyzed using the Mann-Whitney U test. Statistical analysis for experimental data (*in vitro* and *in vivo*) was carried out using GraphPad Prism version 7.0c.

SUPPLEMENTAL INFORMATION

Supplemental Information includes Supplemental Materials and Methods, five figures, one table, and six movie and can be found with this article online at https://doi.org/10.1016/j.ymthe.2018.01.011.

AUTHOR CONTRIBUTIONS

H.J., L.M., and A. Backlund conceived and designed the experiments and analyzed the data. H.J. and D.Y.L. performed *in vivo* experiments and statistics. D.Y.L., A. Backlund, E.C., C.S., A. Busch, S.M.E., P.S.-G., N.S., R.H., G.W., E.E., M.J., J.P., and H.W. performed the *in vitro* and *ex vivo* experiments. I.N.S. and U.R. performed and assisted with micro-dissection laser capture. L.P.M., H.-H.E., and U.H. supported the project with biobank material and expertise in its handling and analysis. H.J., L.M., and A. Backlund wrote the manuscript.

CONFLICTS OF INTEREST

The authors declare that they have no conflict of interest.

ACKNOWLEDGMENTS

This study was supported through funding from the Swedish Heart-Lung-Foundation (20120615, 20130664, and 20140186), the Ragnar Söderberg Foundation (M-14/55), the Karolinska Institute Cardiovascular Program Career Development Grant, the European Research Council (ERC Starting Grant NORVAS), the German Center for Cardiovascular Research (DZHK), the Swedish Research Council (K2009-65X-2233-01-3, K2013-65X-06816-30-4, and 349-2007-8703), Uppdrag Besegra Stroke (P581/2011-123), the Strategic Cardiovascular Programs of Karolinska Institutet and Stockholm County Council (ALF-2011-0260 and ALF-2011-0279), the Foundation for Strategic Research, and the European Commission (CarTarDis, AtheroR-emo, VIA, and AtheroFlux projects).

REFERENCES

1. Mozaffarian, D., Benjamin, E.J., Go, A.S., Arnett, D.K., Blaha, M.J., Cushman, M., Das, S.R., de Ferranti, S., Després, J.P., Fullerton, H.J., et al.; Writing Group Members; American Heart Association Statistics Committee; Stroke Statistics Subcommittee (2016). Heart disease and stroke statistics-2016 update: a report from the American Heart Association. Circulation *133*, e38–e360.
2. Hajifathalian, K., Ueda, P., Lu, Y., Woodward, M., Ahmadvand, A., Aguilar-Salinas, C.A., Azizi, F., Cifkova, R., Di Cesare, M., Eriksen, L., et al. (2015). A novel risk score to predict cardiovascular disease risk in national populations (Globorisk): a pooled analysis of prospective cohorts and health examination surveys. Lancet Diabetes Endocrinol. *3*, 339–355.
3. Gupta, A., Baradaran, H., Schweitzer, A.D., Kamel, H., Pandya, A., Delgado, D., Dunning, A., Mushlin, A.I., and Sanelli, P.C. (2013). Carotid plaque MRI and stroke risk: a systematic review and meta-analysis. Stroke *44*, 3071–3077.
4. Tarkin, J.M., Dweck, M.R., Evans, N.R., Takx, R.A., Brown, A.J., Tawakol, A., Fayad, Z.A., and Rudd, J.H. (2016). Imaging atherosclerosis. Circ. Res. *118*, 750–769.
5. Howard, D.P., van Lammeren, G.W., Rothwell, P.M., Redgrave, J.N., Moll, F.L., de Vries, J.P., de Kleijn, D.P., den Ruijter, H.M., de Borst, G.J., and Pasterkamp, G. (2015). Symptomatic carotid atherosclerotic disease: correlations between plaque composition and ipsilateral stroke risk. Stroke *46*, 182–189.
6. Bentzon, J.F., Otsuka, F., Virmani, R., and Falk, E. (2014). Mechanisms of plaque formation and rupture. Circ. Res. *114*, 1852–1866.
7. van Koeverden, I.D., van Haelst, S.T.W., Haitjema, S., de Vries, J.P.M., Moll, F.L., den Ruijter, H.M., Hoefer, I.E., Dalmeijer, G.W., de Borst, G.J., and Pasterkamp, G. (2017). Time-dependent trends in cardiovascular adverse events during follow-up after carotid or iliofemoral endarterectomy. Br. J. Surg. *104*, 1477–1485.
8. Selwaness, M., Bos, D., van den Bouwhuijsen, Q., Portegies, M.L., Ikram, M.A., Hofman, A., Franco, O.H., van der Lugt, A., Wentzel, J.J., and Vernooij, M.W. (2016). Carotid atherosclerotic plaque characteristics on magnetic resonance imaging relate with history of stroke and coronary heart disease. Stroke *47*, 1542–1547.
9. Dweck, M.R., Aikawa, E., Newby, D.E., Tarkin, J.M., Rudd, J.H., Narula, J., and Fayad, Z.A. (2016). Noninvasive molecular imaging of disease activity in atherosclerosis. Circ. Res. *119*, 330–340.
10. Feinberg, M.W., and Moore, K.J. (2016). MicroRNA regulation of atherosclerosis. Circ. Res. *118*, 703–720.
11. Maegdefessel, L., Azuma, J., Toh, R., Deng, A., Merk, D.R., Raiesdana, A., Leeper, N.J., Raaz, U., Schoelmerich, A.M., McConnell, M.V., et al. (2012). MicroRNA-21 blocks abdominal aortic aneurysm development and nicotine-augmented expansion. Sci. Transl. Med. *4*, 122ra22.
12. Wang, D., Deuse, T., Stubbendorff, M., Chernogubova, E., Erben, R.G., Eken, S.M., Jin, H., Li, Y., Busch, A., Heeger, C.H., et al. (2015). Local microRNA modulation using a novel anti-miR-21-eluting stent effectively prevents experimental in-stent restenosis. Arterioscler. Thromb. Vasc. Biol. *35*, 1945–1953.
13. Albinsson, S., and Sessa, W.C. (2011). Can microRNAs control vascular smooth muscle phenotypic modulation and the response to injury? Physiol. Genomics *43*, 529–533.
14. Stary, H.C., Chandler, A.B., Dinsmore, R.E., Fuster, V., Glagov, S., Insull, W., Jr., Rosenfeld, M.E., Schwartz, C.J., Wagner, W.D., and Wissler, R.W. (1995). A definition of advanced types of atherosclerotic lesions and a histological classification of atherosclerosis. A report from the Committee on Vascular Lesions of the Council on Arteriosclerosis, American Heart Association. Circulation *92*, 1355–1374.
15. Redgrave, J.N., Gallagher, P., Lovett, J.K., and Rothwell, P.M. (2008). Critical cap thickness and rupture in symptomatic carotid plaques: the oxford plaque study. Stroke *39*, 1722–1729.
16. Eken, S.M., Jin, H., Chernogubova, E., Li, Y., Simon, N., Sun, C., Korzunowicz, G., Busch, A., Bäcklund, A., Österholm, C., et al. (2017). MicroRNA-210 enhances fibrous cap stability in advanced atherosclerotic lesions. Circ. Res. *120*, 633–644.
17. Aken, B.L., Achuthan, P., Akanni, W., Amode, M.R., Bernsdorff, F., Bhai, J., Billis, K., Carvalho-Silva, D., Cummins, C., Clapham, P., et al. (2017). Ensembl 2017. Nucleic Acids Res. *45* (D1), D635–D642.
18. Zerbino, D.R., Johnson, N., Juetteman, T., Sheppard, D., Wilder, S.P., Lavidas, I., Nuhn, M., Perry, E., Raffaillac-Desfosses, Q., Sobral, D., et al. (2016). Ensembl regulation resources. Database (Oxford) *2016*, bav119.
19. Ram, R.R., Mendiratta, S., Bodemann, B.O., Torres, M.J., Eskiocak, U., and White, M.A. (2014). RASSF1A inactivation unleashes a tumor suppressor/oncogene cascade with context-dependent consequences on cell cycle progression. Mol. Cell. Biol. *34*, 2350–2358.
20. Singh, S.K., Kagalwala, M.N., Parker-Thornburg, J., Adams, H., and Majumder, S. (2008). REST maintains self-renewal and pluripotency of embryonic stem cells. Nature *453*, 223–227.
21. Ji, R., Cheng, Y., Yue, J., Yang, J., Liu, X., Chen, H., Dean, D.B., and Zhang, C. (2007). MicroRNA expression signature and antisense-mediated depletion reveal an essential role of MicroRNA in vascular neointimal lesion formation. Circ. Res. *100*, 1579–1588.
22. Gandhi, C., Khan, M.M., Lentz, S.R., and Chauhan, A.K. (2012). ADAMTS13 reduces vascular inflammation and the development of early atherosclerosis in mice. Blood *119*, 2385–2391.
23. Feng, J., Li, A., Deng, J., Yang, Y., Dang, L., Ye, Y., Li, Y., and Zhang, W. (2014). miR-21 attenuates lipopolysaccharide-induced lipid accumulation and inflammatory response: potential role in cerebrovascular disease. Lipids Health Dis. *13*, 27.
24. Bang, C., Batkai, S., Dangwal, S., Gupta, S.K., Foinquinos, A., Holzmann, A., Just, A., Remke, J., Zimmer, K., Zeug, A., et al. (2014). Cardiac fibroblast-derived microRNA passenger strand-enriched exosomes mediate cardiomyocyte hypertrophy. J. Clin. Invest. *124*, 2136–2146.
25. Thum, T., Gross, C., Fiedler, J., Fischer, T., Kissler, S., Bussen, M., Galuppo, P., Just, S., Rottbauer, W., Frantz, S., et al. (2008). MicroRNA-21 contributes to myocardial disease by stimulating MAP kinase signalling in fibroblasts. Nature *456*, 980–984.
26. McDonald, R.A., Halliday, C.A., Miller, A.M., Diver, L.A., Dakin, R.S., Montgomery, J., McBride, M.W., Kennedy, S., McClure, J.D., Robertson, K.E., et al. (2015). Reducing in-stent restenosis: therapeutic manipulation of miRNA in vascular remodeling and inflammation. J. Am. Coll. Cardiol. *65*, 2314–2327.
27. Raitoharju, E., Lyytikäinen, L.P., Levula, M., Oksala, N., Mennander, A., Tarkka, M., Klopp, N., Illig, T., Kähönen, M., Karhunen, P.J., et al. (2011). miR-21, miR-210, miR-34a, and miR-146a/b are up-regulated in human atherosclerotic plaques in the Tampere Vascular Study. Atherosclerosis *219*, 211–217.
28. Wei, Y., Schober, A., and Weber, C. (2013). Pathogenic arterial remodeling: the good and bad of microRNAs. Am. J. Physiol. Heart Circ. Physiol. *304*, H1050–H1059.
29. Canfrán-Duque, A., Rotllan, N., Zhang, X., Fernández-Fuertes, M., Ramírez-Hidalgo, C., Araldi, E., Daimiel, L., Busto, R., Fernández-Hernando, C., and Suárez, Y. (2017). Macrophage deficiency of miR-21 promotes apoptosis, plaque necrosis, and vascular inflammation during atherogenesis. EMBO Mol. Med. *9*, 1244–1262.
30. Yin, M., Yuan, Y., Cui, Y., Hong, X., Luo, H., Hu, X., Tang, M., Hescheler, J., and Xi, J. (2015). Puerarin suppresses the self-renewal of murine embryonic stem cells by inhibition of REST-MiR-21 regulatory pathway. Cell. Physiol. Biochem. *37*, 527–536.
31. Singh, S.K., Marisetty, A., Sathyan, P., Kagalwala, M., Zhao, Z., and Majumder, S. (2015). REST-miR-21-SOX2 axis maintains pluripotency in E14Tg2a.4 embryonic stem cells. Stem Cell Res. (Amst.) *15*, 305–311.
32. Mendell, J.T., and Olson, E.N. (2012). MicroRNAs in stress signaling and human disease. Cell *148*, 1172–1187.
33. Bergsland, M., Covacu, R., Perez Estrada, C., Svensson, M., and Brundin, L. (2014). Nitric oxide-induced neuronal to glial lineage fate-change depends on NRSF/REST function in neural progenitor cells. Stem Cells *32*, 2539–2549.
34. Meng, F., Henson, R., Wehbe-Janek, H., Ghoshal, K., Jacob, S.T., and Patel, T. (2007). MicroRNA-21 regulates expression of the PTEN tumor suppressor gene in human hepatocellular cancer. Gastroenterology *133*, 647–658.
35. Meng, F., Henson, R., Lang, M., Wehbe, H., Maheshwari, S., Mendell, J.T., Jiang, J., Schmittgen, T.D., and Patel, T. (2006). Involvement of human micro-RNA in growth and response to chemotherapy in human cholangiocarcinoma cell lines. Gastroenterology *130*, 2113–2129.
36. Dey, N., Ghosh-Choudhury, N., Kasinath, B.S., and Choudhury, G.G. (2012). TGFβ-stimulated microRNA-21 utilizes PTEN to orchestrate AKT/mTORC1 signaling for mesangial cell hypertrophy and matrix expansion. PLoS ONE *7*, e42316.

37. Shin, V.Y., Jin, H., Ng, E.K., Cheng, A.S., Chong, W.W., Wong, C.Y., Leung, W.K., Sung, J.J., and Chu, K.M. (2011). NF-κB targets miR-16 and miR-21 in gastric cancer: involvement of prostaglandin E receptors. Carcinogenesis *32*, 240–245.

38. Wei, C., Li, L., Kim, I.K., Sun, P., and Gupta, S. (2014). NF-κB mediated miR-21 regulation in cardiomyocytes apoptosis under oxidative stress. Free Radic. Res. *48*, 282–291.

39. Romay, M.C., Che, N., Becker, S.N., Pouldar, D., Hagopian, R., Xiao, X., Lusis, A.J., Berliner, J.A., and Civelek, M. (2015). Regulation of NF-κB signaling by oxidized glycerophospholipid and IL-1β induced miRs-21-3p and -27a-5p in human aortic endothelial cells. J. Lipid Res. *56*, 38–50.

40. Rupaimoole, R., and Slack, F.J. (2017). MicroRNA therapeutics: towards a new era for the management of cancer and other diseases. Nat. Rev. Drug Discov. *16*, 203–222.

41. van Rooij, E., and Kauppinen, S. (2014). Development of microRNA therapeutics is coming of age. EMBO Mol. Med. *6*, 851–864.

42. Dangwal, S., and Thum, T. (2014). microRNA therapeutics in cardiovascular disease models. Annu. Rev. Pharmacol. Toxicol. *54*, 185–203.

43. Maegdefessel, L. (2014). The emerging role of microRNAs in cardiovascular disease. J. Intern. Med. *276*, 633–644.

44. McClelland, A.D., Herman-Edelstein, M., Komers, R., Jha, J.C., Winbanks, C.E., Hagiwara, S., et al. (2015). miR-21 promotes renal fibrosis in diabetic nephropathy by targeting PTEN and SMAD7. Clin. Sci. *129*, 1237–1249.

45. Gong, C., Yao, Y., Wang, Y., Liu, B., Wu, W., Chen, J., Su, F., Yao, H., and Song, E. (2011). Up-regulation of miR-21 mediates resistance to trastuzumab therapy for breast cancer. J. Biol. Chem. *286*, 19127–19137.

46. Seike, M., Goto, A., Okano, T., Bowman, E.D., Schetter, A.J., Horikawa, I., Mathe, E.A., Jen, J., Yang, P., Sugimura, H., et al. (2009). MiR-21 is an EGFR-regulated anti-apoptotic factor in lung cancer in never-smokers. Proc. Natl. Acad. Sci. U S A *106*, 12085–12090.

47. Thurnherr, T., Mah, W.C., Lei, Z., Jin, Y., Rozen, S.G., and Lee, C.G. (2016). Differentially expressed miRNAs in hepatocellular carcinoma target genes in the genetic information processing and metabolism pathways. Sci. Rep. *6*, 20065.

48. Tang, K., and Xu, H. (2015). Prognostic value of meta-signature miRNAs in renal cell carcinoma: an integrated miRNA expression profiling analysis. Sci. Rep. *5*, 10272.

49. Kadera, B.E., Li, L., Toste, P.A., Wu, N., Adams, C., Dawson, D.W., and Donahue, T.R. (2013). MicroRNA-21 in pancreatic ductal adenocarcinoma tumor-associated fibroblasts promotes metastasis. PLoS ONE *8*, e71978.

50. Mulder, W.J., Jaffer, F.A., Fayad, Z.A., and Nahrendorf, M. (2014). Imaging and nanomedicine in inflammatory atherosclerosis. Sci. Transl. Med. *6*, 239sr1.

51. Cao, W.J., Rosenblat, J.D., Roth, N.C., Kuliszewski, M.A., Matkar, P.N., Rudenko, D., Liao, C., Lee, P.J., and Leong-Poi, H. (2015). Therapeutic angiogenesis by ultrasound-mediated microRNA-126-3p delivery. Arterioscler. Thromb. Vasc. Biol. *35*, 2401–2411.

52. Kwekkeboom, R.F., Lei, Z., Bogaards, S.J., Aiazian, E., Kamp, O., Paulus, W.J., Sluijter, J.P., and Musters, R.J. (2015). Ultrasound and microbubble-induced local delivery of microRNA-based therapeutics. Ultrasound Med. Biol. *41*, 163–176.

53. Carson, A.R., McTiernan, C.F., Lavery, L., Grata, M., Leng, X., Wang, J., Chen, X., and Villanueva, F.S. (2012). Ultrasound-targeted microbubble destruction to deliver siRNA cancer therapy. Cancer Res. *72*, 6191–6199.

54. Stigliano, C., Ramirez, M.R., Singh, J.V., Aryal, S., Key, J., Blanco, E., and Decuzzi, P. (2017). Methotraxate-loaded hybrid nanoconstructs target vascular lesions and inhibit atherosclerosis progression in ApoE-/- mice. Adv. Healthc. Mater. *6*, 6.

55. Ma, X., Kumar, M., Choudhury, S.N., Becker Buscaglia, L.E., Barker, J.R., Kanakamedala, K., Liu, M.F., and Li, Y. (2011). Loss of the miR-21 allele elevates the expression of its target genes and reduces tumorigenesis. Proc. Natl. Acad. Sci. U S A *108*, 10144–10149.

56. Shankman, L.S., Gomez, D., Cherepanova, O.A., Salmon, M., Alencar, G.F., Haskins, R.M., Swiatlowska, P., Newman, A.A., Greene, E.S., Straub, A.C., et al. (2015). KLF4-dependent phenotypic modulation of smooth muscle cells has a key role in atherosclerotic plaque pathogenesis. Nat. Med. *21*, 628–637.

57. Kumar, A., and Lindner, V. (1997). Remodeling with neointima formation in the mouse carotid artery after cessation of blood flow. Arterioscler. Thromb. Vasc. Biol. *17*, 2238–2244.

58. Sasaki, T., Kuzuya, M., Nakamura, K., Cheng, X.W., Shibata, T., Sato, K., and Iguchi, A. (2006). A simple method of plaque rupture induction in apolipoprotein E-deficient mice. Arterioscler. Thromb. Vasc. Biol. *26*, 1304–1309.

59. Magné, J., Gustafsson, P., Jin, H., Maegdefessel, L., Hultenby, K., Wernerson, A., Eriksson, P., Franco-Cereceda, A., Kovanen, P.T., Gonçalves, I., and Ehrenborg, E. (2015). ATG16L1 expression in carotid atherosclerotic plaques is associated with plaque vulnerability. Arterioscler. Thromb. Vasc. Biol. *35*, 1226–1235.

60. Kuhlmann, M.T., Cuhlmann, S., Hoppe, I., Krams, R., Evans, P.C., Strijkers, G.J., Nicolay, K., Hermann, S., and Schäfers, M. (2012). Implantation of a carotid cuff for triggering shear-stress induced atherosclerosis in mice. J. Vis. Exp. (59), 3308.

61. Jin, S.X., Shen, L.H., Nie, P., Yuan, W., Hu, L.H., Li, D.D., Chen, X.J., Zhang, X.K., and He, B. (2012). Endogenous renovascular hypertension combined with low shear stress induces plaque rupture in apolipoprotein E-deficient mice. Arterioscler. Thromb. Vasc. Biol. *32*, 2372–2379.

62. Bot, I., de Jager, S.C., Bot, M., van Heiningen, S.H., de Groot, P., Veldhuizen, R.W., van Berkel, T.J., von der Thüsen, J.H., and Biessen, E.A. (2010). The neuropeptide substance P mediates adventitial mast cell activation and induces intraplaque hemorrhage in advanced atherosclerosis. Circ. Res. *106*, 89–92.

63. Liu, Y., Li, L., Su, Q., Liu, T., Ma, Z., and Yang, H. (2015). Ultrasound-targeted microbubble destruction enhances gene expression of microRNA-21 in swine heart via intracoronary delivery. Echocardiography *32*, 1407–1416.